CDF/DOC/CALORIMETRY/CDFR/5926
August 13, 2002
VERSION 1.0

Missing E_T and Beam related backgrounds at CDF

M. Albrow, C.M. Ginsburg, B. Heinemann, S. Lee, K. Maeshima, P. Murat, V. Papadimitriou, C. Pilcher, K. Terashi, R.J. Tesarek, J. Thom

Abstract

We have studied the features of beam-induced background events at CDF with large missing E_T. These events contribute to a relatively large missing E_T trigger rate, and may produce an irreducible background to some missing E_T physics signatures. The energy deposition of these events falls into two classes. In one class, the events have large energy depositions localized at $\phi \approx 0°$ in the CDF calorimeters (missing E_T peaking at $\phi \approx 180°$) and they usually have signals in several η towers in a row mainly in the central calorimeter. The events have no COT tracks associated with the calorimeter showers and may leave hits in the toroid scintillator of the IMU intermediate muon chamber system. The rate of these events increases when the CDF roman pot detectors are inserted into the beam line. In the other class, the events deposit a significant amount of energy at the highest η towers of the plug CDF calorimeters, closest to the beam. Our current knowledge of background sources is described.

Contents

1 Introduction **3**

2 Missing E_T Peaking at $\phi \approx 180°$ **3**
2.1 Origin of the Muons 10
2.2 The Effect of the Roman Pots 13

3 Missing E_T Peaking at $\phi \approx 90°, 270°$ **20**
3.1 Collision data 20
3.2 Proton-only Stores 23

4 Conclusion **26**

5 Comments on Beam Halo - Plans **27**

6 Appendix: Roman Pot Scan of August 1st 2002 **34**

1 Introduction

In this note we describe two classes of CDF events which seem to originate from the Beam Halo. Both classes have large missing E_T and exhibit interesting features in the ϕ distribution for the missing E_T of the event. Figure 1 shows the ϕ distribution of the missing E_T vector in collision events taken with the W-No-Track trigger [1]. These events contribute to higher missing E_T trigger rates and may produce an irreducible background to some high missing E_T physics signatures like SUSY searches, gauge mediated interactions, etc. In one category of events we see a prominent peak in the missing E_T distribution at $\phi \approx 180°$ which corresponds to showers at $\phi \approx 0°$ (0°-15° and 345°-360°), the outside (N) of CDF. In the other category we see prominent peaks in the missing E_T distribution at $\phi \approx 90°$ and $\phi \approx 270°$ which corresponds to showers at the highest η towers of the plug calorimeters. Note that in the CDF coordinate system ϕ is measured on the plane transverse to the beam and increases clockwise from the North to the South as we face the East. Note that protons go from West to East.

2 Missing E_T Peaking at $\phi \approx 180°$

The events we will describe below come from a stripping of Stream E data (jets) for runs 141432-141440 with the requirement that the missing E_T of the event is greater than 50 GeV, and we will refer to them as the *MET* events from now on.

In Figures 2 and 3 we show the calorimeter and COT views of two CDF *MET* events. They have showers occupying several η towers in a row at $\phi \approx 0°$ and usually one or two of these η towers have a large energy deposition. We observe that for the central calorimeter the energy in each η tower for these events is either only electromagnetic or only hadronic and almost never a mixture of both electromagnetic and hadronic energies. Since the Central ElectroMagnetic (CEM) calorimeter is relatively long and thin (see Figure 4), the particles producing these events must be traveling roughly parallel to the CDF axis. In addition to the energy in the central calorimeters there is often energy at the same ϕ in the Wall (WHA) and Plug (PHA) HAdronic calorimeters as well. We also observe that there are almost never COT tracks associated with the energy depositions in these events. This indicates that

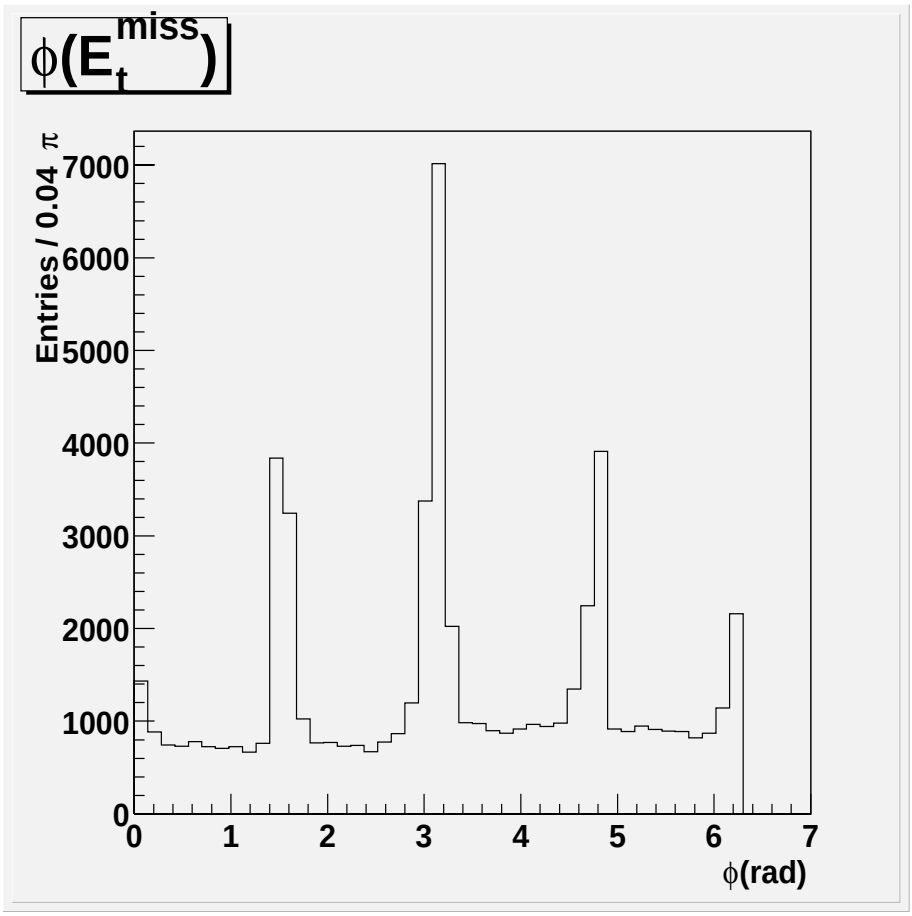

Figure 1: The ϕ distribution of the missing E_T in W-No-Track collision events for runs 138425 to 141212.

the events under discussion do not come from the interaction region and probably travel almost parallel to the beam line.

Figure 5 shows the energy distribution in the $\eta - \phi$ plane of the MET events. We observe that the majority of these events have $\phi \approx 0°$ corresponding to $iphi = 0$ or $iphi = 23$ in the CDF calorimetry tower indexing. The events also appear to be distributed symmetrically in η around $ieta = 26$. Note that for the central calorimeters ($|\eta|$ <1.10) we have one calorimeter tower for $\Delta\phi = 15°$ while for the plug calorimeters we have one calorimeter tower within $\Delta\phi = 15°$ for 2.11< $|\eta|$ <3.49 and two towers, of 7.5° each, for 1.10< $|\eta|$ <2.11.

In Figure 6 we show the timing distribution for events with missing $E_T <$ 30 GeV, as well as for the MET events (missing $E_T > 50$ GeV). The timing is measured with the TDC counters connected to the hadronic calorimeters. We observe that for events with missing $E_T < 30$ GeV the distribution peaks at about 1 ns while for the MET events the distribution peaks at about -7 ns. This indicates that the MET events arrive earlier than normal collision events and therefore they do not originate from the interaction point.

In Figure 7 we show the time difference between events in the East and events in the West. The timing is measured again with the TDCs of the hadronic calorimeters. We observe that for events with missing $E_T < 30$ GeV the time difference peaks around 1 ns while for events with missing $E_T > 50$ GeV it peaks around 10 ns. The time difference is consistent with the distance between the faces of the East and West calorimeters. This indicates that the events come from the West.

In Figure 8 we show the timing distribution in ns for the MET events for the West and East Toroid Scintillator Intermediate Muon Counters (TSU). These counters have a granularity of 5° in ϕ and cover the pseudorapidity range 1.3 - 1.5. Note that the occupancy in the West is higher than the occupancy in the East. The difference in time for the peaks of the distributions between West and East is about 40 ns, consistent with the distance between West and East TSU. This indicates that the above events come from the West, the direction of the protons, in time with the proton beam.

In Figure 9 we show the TSU counter occupancy distribution for the MET events which are in time with the proton beam for the West and East TSU counters. The timing cuts on the TSU counters for events that enter Figure 9 are 50 ns for both East and West. For the West TSU we require $100 < t < 150$ ns while for the East TSU we require $140 < t < 190$ ns.

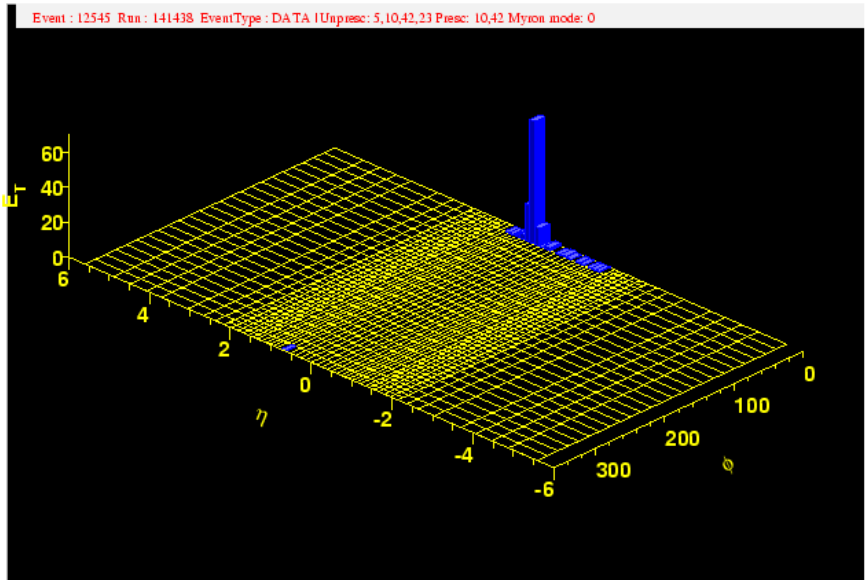

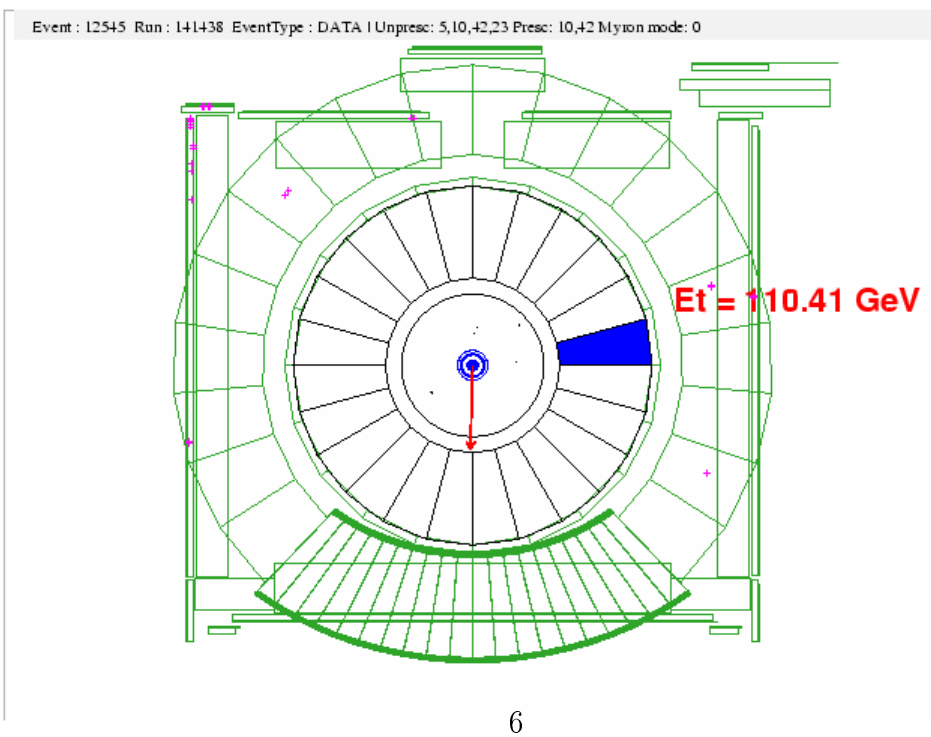

Figure 2: Calorimeter view (top) and COT view (bottom) of event 12545 in run 141438. For the calorimetry view picture, North is to the right. The arrow in the COT view represents the missing E_T vector but it was wrong by 90° at the time these snapshots were taken.

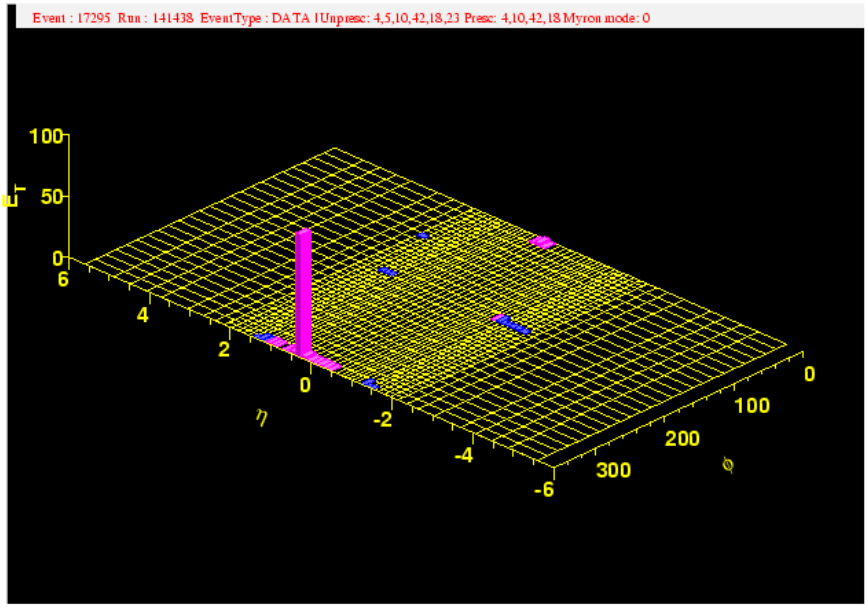

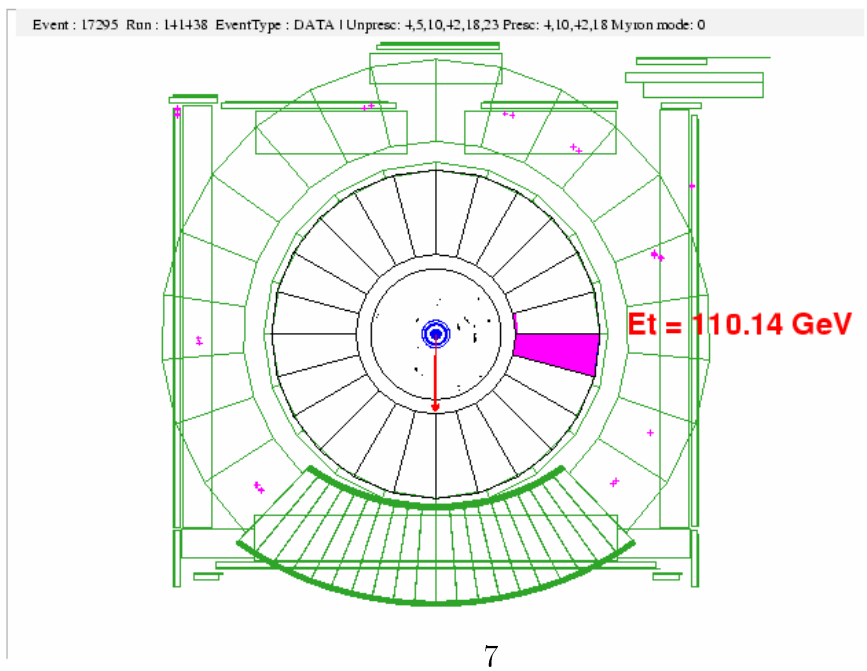

Figure 3: Calorimeter view (top) and COT view (bottom) of event 17295 in run 141438.

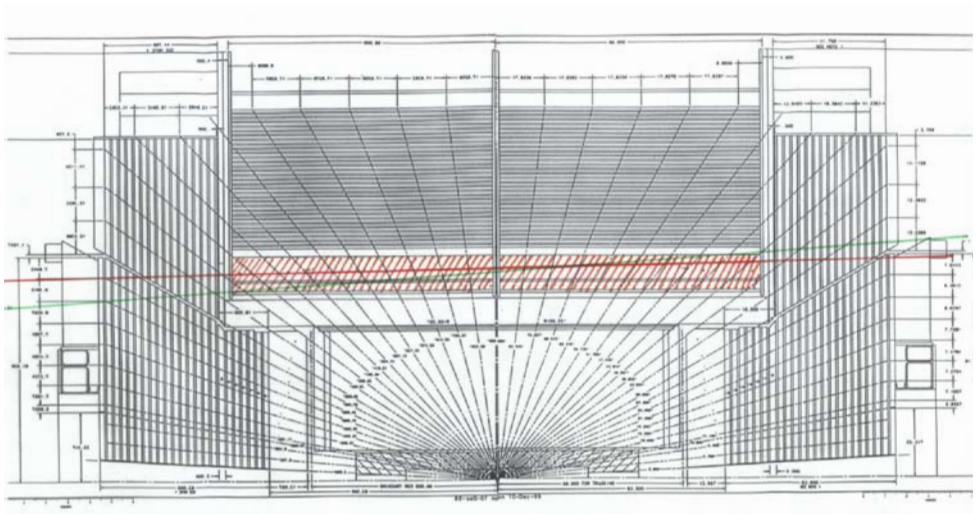

Figure 4: Schematic of the CDF calorimeter systems. The region with the horizontal parallel lines indicates the Central Hadronic calorimeter (CHA). The hatched region indicates the Central Electromagnetic calorimeter (CEM). The vertical parallel lines indicate the Plug Electromagnetic (PEM) and Hadronic (PHA) calorimeters and the Wall Hadronic (WHA) calorimeter. The two lines crossing the CEM calorimeter indicate the minimum and maximum angles at which a charged particle originating from the proton beam line may pass through only the CEM calorimeter. West is to the left in this figure and protons come from the left.

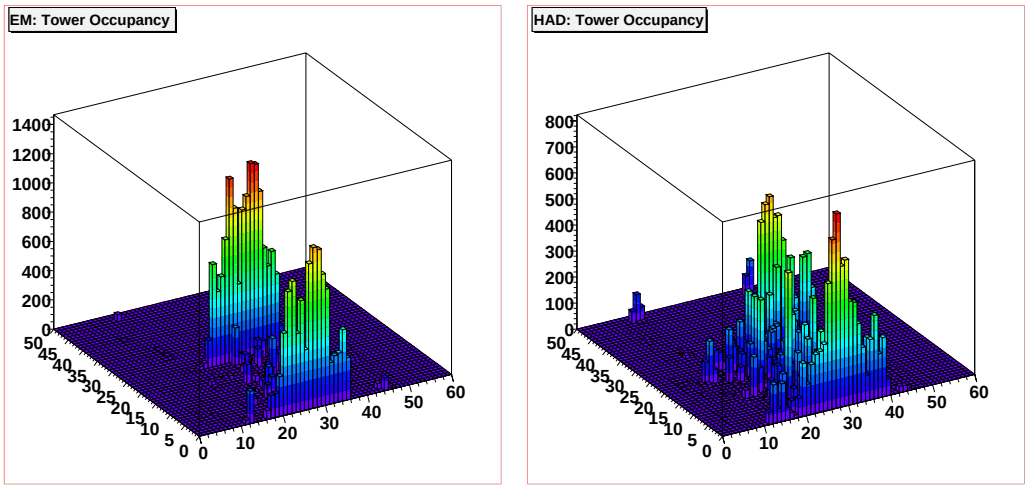

Figure 5: Tower occupancy distribution in the $\eta - \phi$ plane for events with missing $E_T > 50$ GeV. (left) Electromagnetic calorimeters; (right) Hadronic calorimeters. (η is left-right, ϕ is front-back).

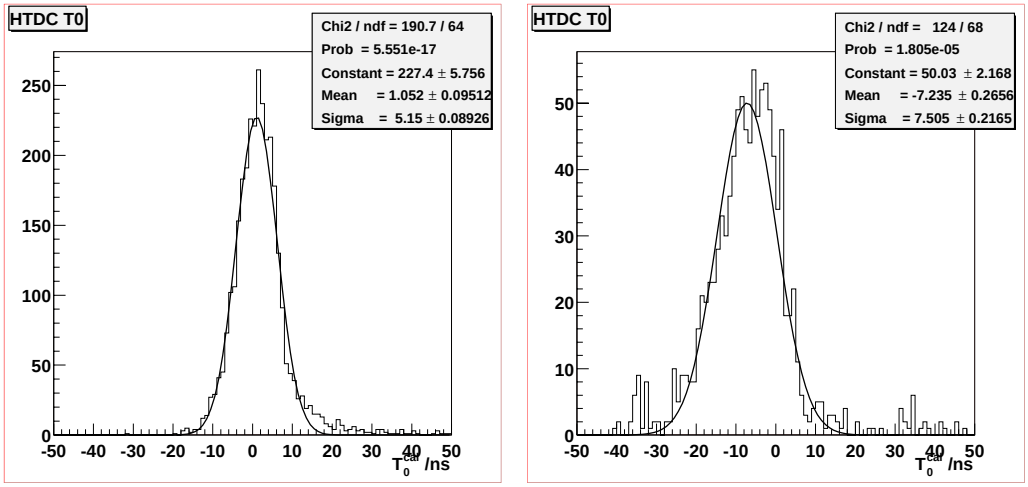

Figure 6: Time distribution in the hadronic calorimeters for events with missing $E_T < 30$ GeV (left) and missing $E_T > 50$ GeV (right).

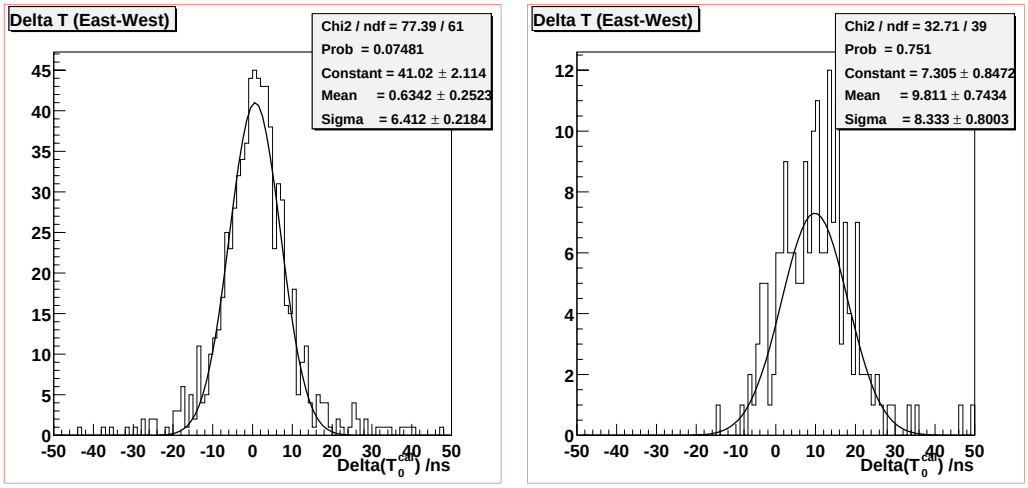

Figure 7: Distribution of the time difference between East and West for events with missing $E_T < 30$ GeV (left); missing $E_T > 50$ GeV (right). The timing is measured with the TDCs of the hadronic calorimeters.

We observe that for the East counters the events are well collimated and located mostly at $\phi \approx 0°$ while for the West counters the events are less collimated and located mostly in the range $\phi = 110° - 180°$. Only 8 events out of the 1000 have both TSU-East and TSU-West hits, and their ϕ's are uncorrelated. Large energy depositions at the central hadronic calorimeter are well correlated in ϕ with the East TSU. The event distribution at the West TSU counters is not yet fully understood.

The above indicate that there are muons associated with the MET events under discussion. These muons do not come from the interaction region, they come almost parallel to the beam line, they move from the West to the East and they are located at $\phi \approx 0°$ at the West and East calorimeters and at the East TSU.

2.1 Origin of the Muons

As discussed earlier, in scanning through many of these events, one finds that they come almost parallel to the CDF beam axis. However, one can estimate the angle that a muon would pass through the CEM calorimeter by counting and comparing the number of hadronic towers with energy on East

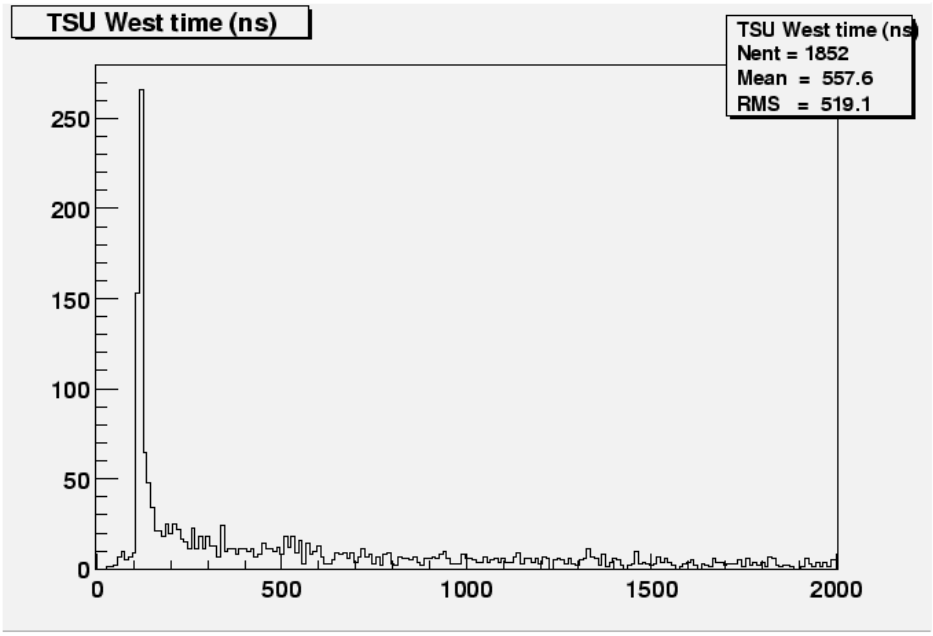

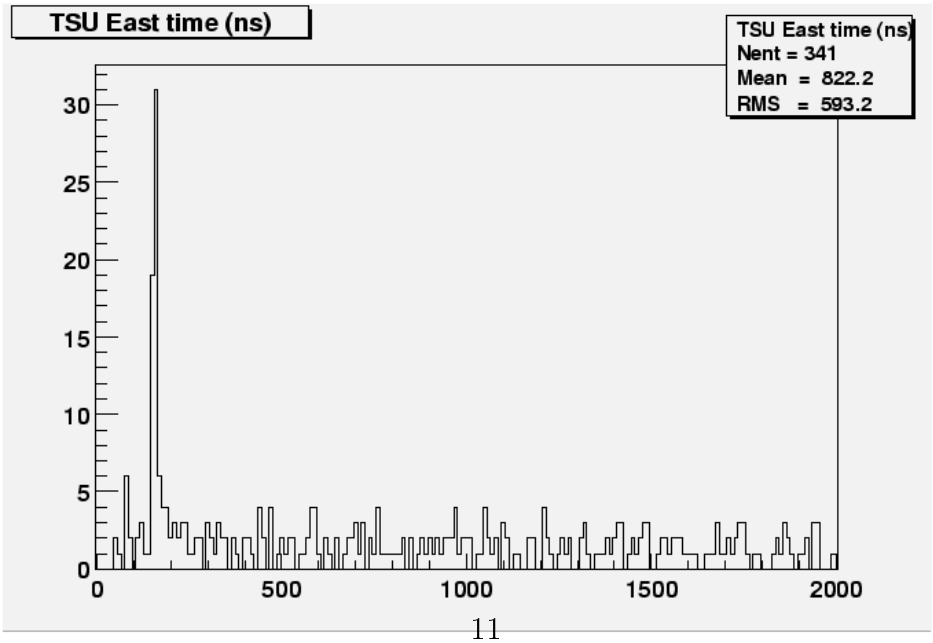

Figure 8: TSU timing distribution in ns for the MET events (top) west TSU; (bottom) east TSU. The bins are 10 ns wide.

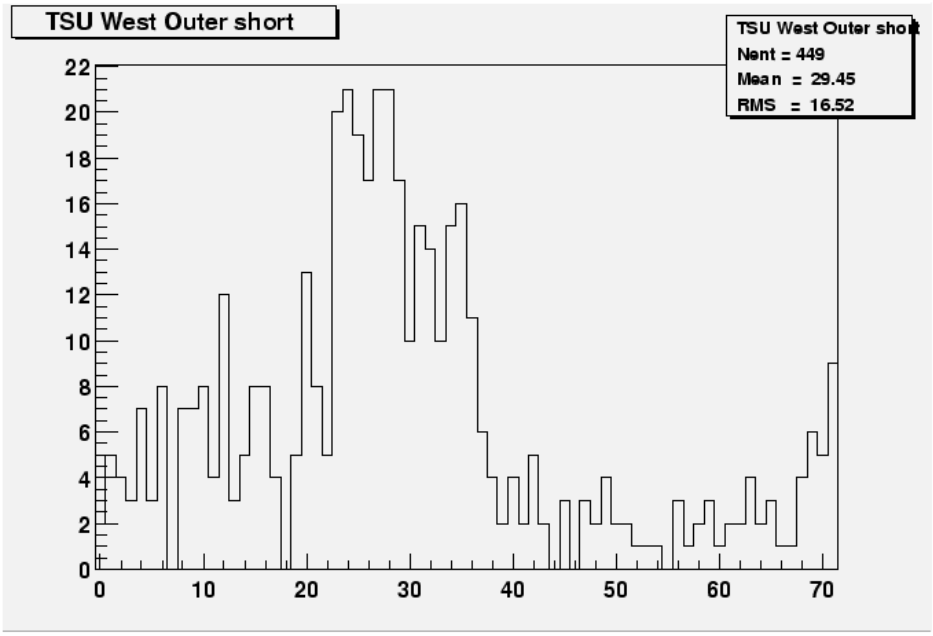

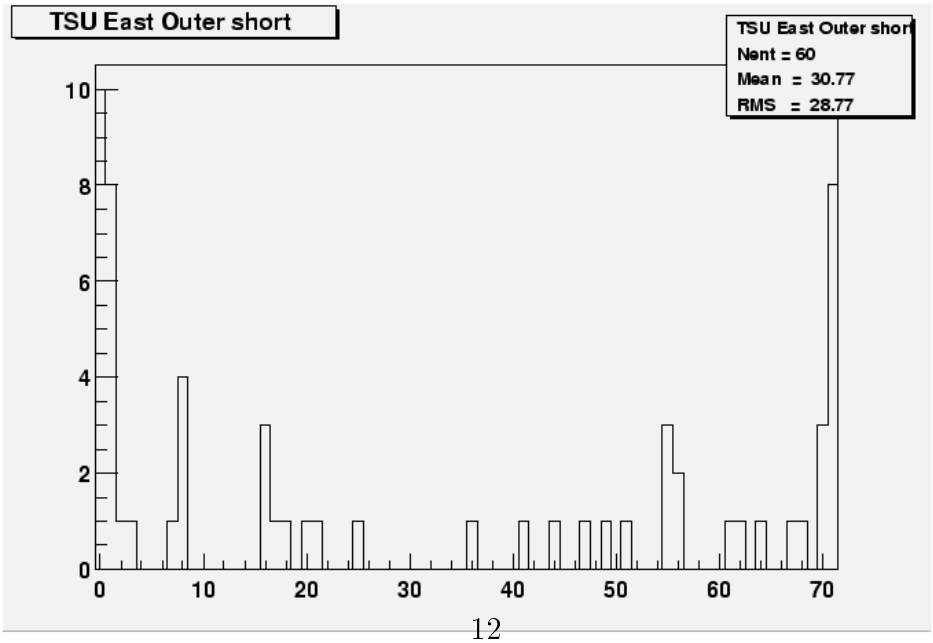

Figure 9: TSU occupancy in ϕ (counter number) of hits in time with the proton beam for the MET events. (top) west TSU; (bottom) east TSU. Each counter spans 5° in ϕ and counter 0 starts at 0° degrees.

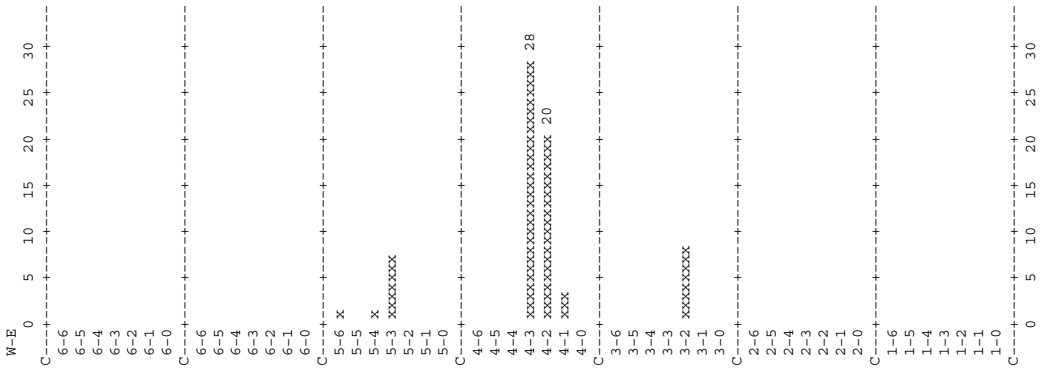

Figure 10: Histogram of different CEM event topologies. The horizontal axis denotes the number of west-east (#W - #E) hadronic towers with energy.

and West of the central calorimeters. (We have assumed here straight line muon trajectories). Figure 4 indicates the minimum and maximum angles one would expect for a muon passing through only the EM portion of the central calorimeters. The minimum angle in the figure represents muons originating farthest to the West of CDF (-81 m) and containing 4 West plug and wall hadronic towers and 3 East plug and wall hadronic towers. The maximum angle in the figure represents muons originating closest to CDF (-24 m) and containing 4 west plug and wall hadronic towers and 2 east plug and wall hadronic towers. Figure 10 shows the results of classifying events as indicated above. A weighted average of the different classes of events yields a point source at -57 ± 5 m. This is in good agreement with the position of the CDF roman pots.

2.2 The Effect of the Roman Pots

After we inserted the roman pot detectors in the beam in store 1113, run 141433, the ϕ distribution for missing $E_T > 45$ GeV exhibited a prominent peak at $\phi \approx 180°$. Note the difference in the ϕ distribution of the missing E_T in Figures 11 and 12 with Pots IN and OUT respectively.

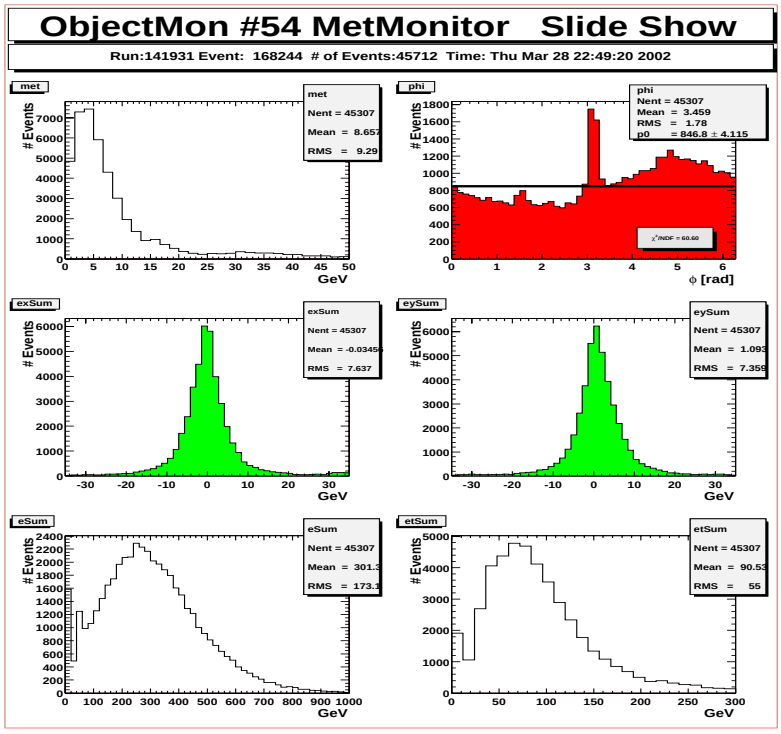

Figure 11: Various distributions for events satisfying the missing E_T trigger for Run 141931. The roman pots are fully inserted.

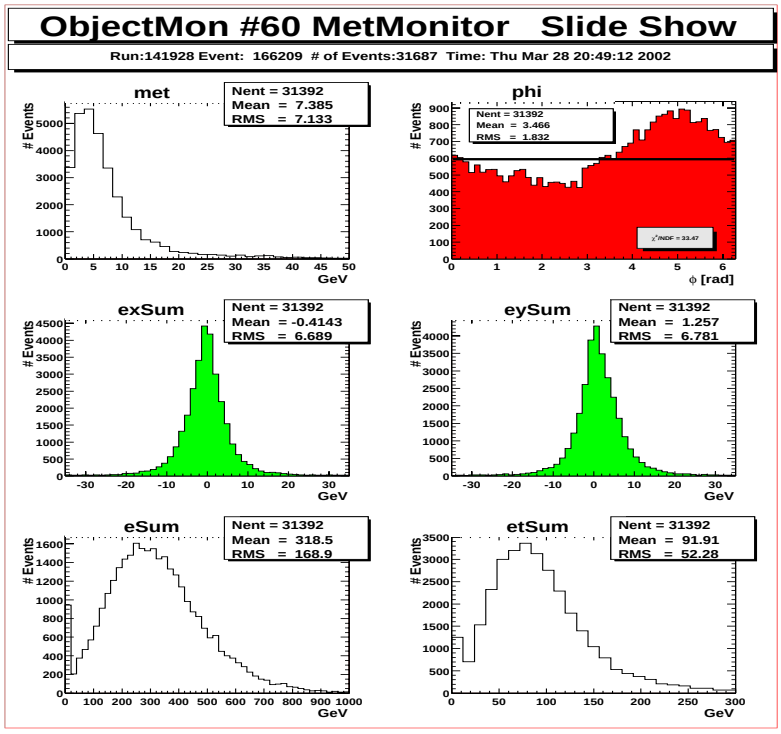

Figure 12: Various distributions for events satisfying the missing E_T trigger for Run 141928. The Roman Pots are completely OUT.

On April 1st, 2002 we performed additional studies varying the roman pot position at the end of colliding beam store 1152, when the luminosity was about 3.5 E30 $cm^{-2}s^{-1}$. As discussed earlier, we observed background events with large missing E_T (satisfying the MET 35 2J and MET 45 triggers). These events correspond to background showers between 0°-15° and 345°-360° and seem to be correlated with whether the roman pot detectors are "close to the beam" or within their "garage" position. "Close to the beam" means with the inside edge of the pot $\sim$ 12 mm from the beam pipe center. In the "garage" position they are retracted to be flush with (or a little behind) the inner edge of the beam pipe. Proton beam halo hitting the pots can interact and send reaction products in the direction of the B0 Interaction Region. There are three pots at about 55, 56 and 57 m west from B0. Between the pots and the CDF detector there are three Tevatron dipoles (each 2.43 m long), 9.3 m of electrostatic separators and 15.8 m of quadrupoles. In this study, the roman pots were moved from the garage position to the IN position in five steps (a total of five positions). For each step the L3 cross sections of the MET35 2J and MET45 triggers were measured. Figure 13 shows the cross sections as a function of pot position integrated over ϕ. Pictures were taken of the ϕ distribution of the MET. Figure 14 shows three examples for MET45.

In the fully OUT position (-864, -853, -854 mils), although the statistics are modest, one sees what is basically a flat distribution with a small enhancement at $\phi \approx 180°$. As discussed earlier this corresponds to background showers in the horizontal plane to the outside of the detector (N). When the pots move in, this spike begins to dominate the distribution; the flat part does not change (it decreases only relatively, not absolutely). We count the events in the spike and elsewhere, and plot the two vs pot position in Figure 15. It can be seen that the flat ϕ part is rather independent of pot position. Presumably this is due mainly to beam halo-pipe collisions upstream (for protons) of CDF. The $\phi \approx 180°$ peak becomes dominant only for the fully IN position ($+176$, $+192$, $+215$ mils), contributing about 1/4 to 1/3 of the rate at intermediate positions. The nominal position for the pots since they started being IN by default is around 0 mils, where the background they generate is significant but not dominant.

In the Appendix, we report on additional studies with collision data taken on August 1, 2002 during a roman pot scan.

From sections 2.1, 2.2 and the Appendix we conclude that a significant

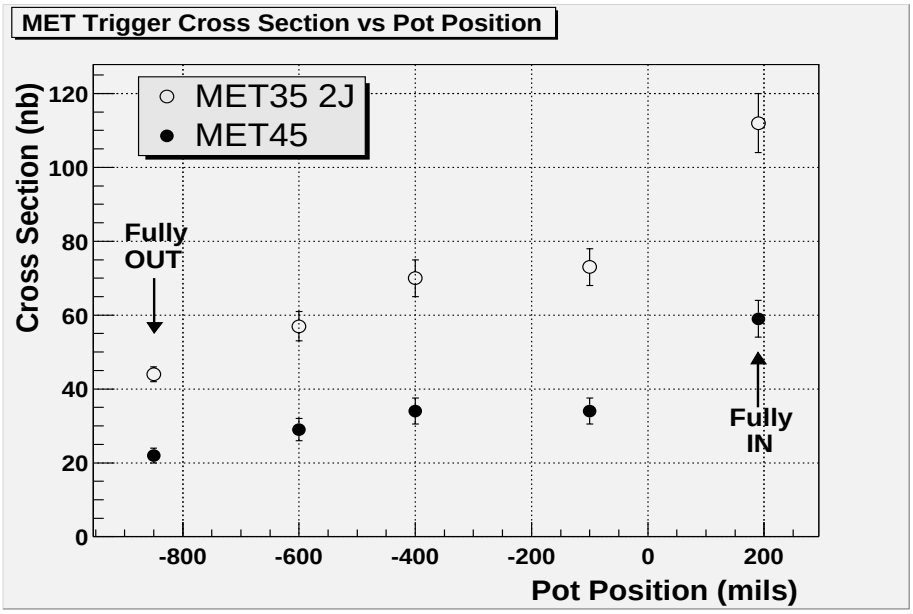

Figure 13: Cross section (integrated over ϕ) in nb vs pot position.

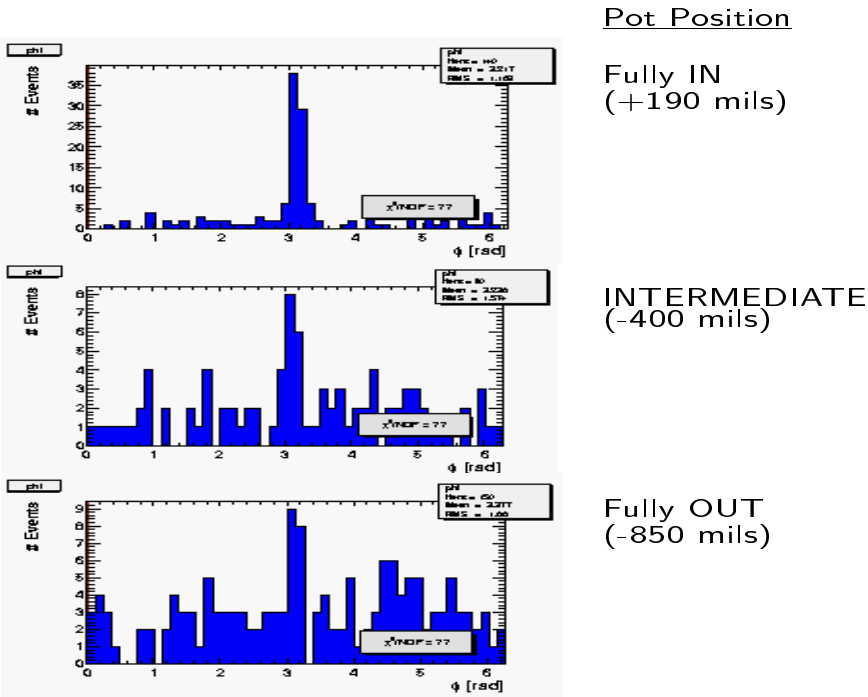

Figure 14: ϕ distribution of the missing E_T for three different positions of the roman pots for the $MET45$ trigger.

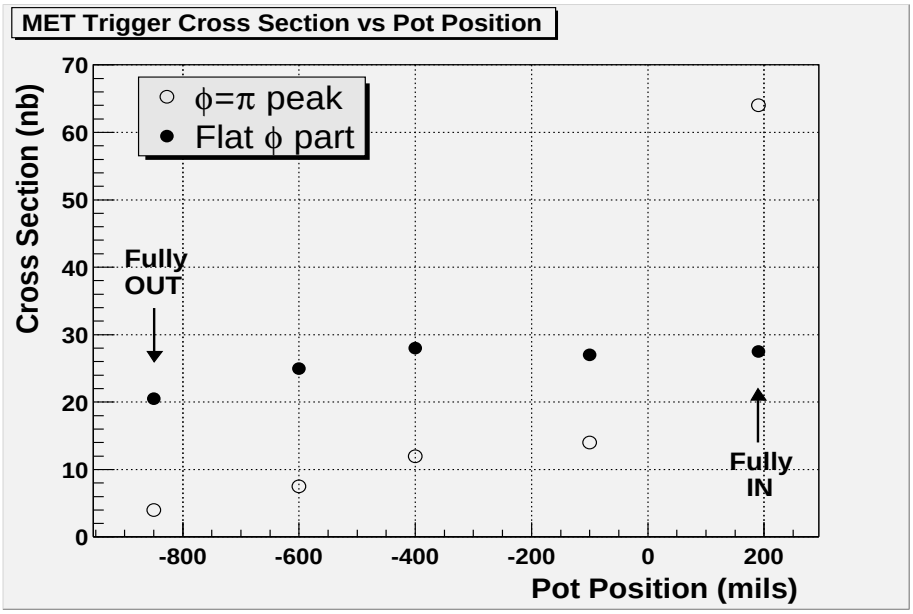

Figure 15: Cross section in nb for the $MET45$ trigger vs pot position. The white circles correspond to the $\phi \approx 180°$ peak. The black circles correspond to all other angles.

fraction of the muons associated with the central calorimeter missing E_T spikes originate at approximately the CDF roman pot location and that the associated background increases as the roman pots move closer to the beam. We also observe that the flat (in ϕ) component is present even when the roman pots are in the "garage" position (see Figure 15).

3 Missing E_T Peaking at $\phi \approx 90°, 270°$

3.1 Collision data

In Figure 16 we show the ϕ distribution of the missing E_T separately for the central, East plug and West plug calorimeters. We have required calorimeter tower geometry cuts to plot the different regions. The central calorimeter requires $17 < ieta < 34$ and the East (West) plug require $ieta > 33 (< 18)$ respectively.

Note that the size of the peaks in the plugs compared with the "flat" background are of the order 10(West):1(East). This is approximately the scaling of the proton/antiproton beam currents. These data suggest that the size of the missing E_T peaks for the plug components in the East/West scale with the proton/antiproton beam currents and are likely due to losses. Timing information from the East and West hadronic calorimeter TDCs could shed more light into this issue. If this is true, it would indicate that the missing E_T related backgrounds we see at the central and plug calorimeters have different sources.

The intermediate shielding walls (intermediate muon system IMU steel) are split vertically along the beam axis. This split produces a gap of approximately 4 cm between the two halves of the IMU steel. A steel "Fin" was added to cover the gap between the two halves of the IMU steel. Figure 17 shows a vertical cross section of the CDF detector and intermediate shielding. This "Fin" is approximately half the thickness of the IMU steel on either side of the gap. Some fraction of the beam halo particles which would normally be stopped by the IMU steel are allowed to pass on to the plug and endwall calorimeters only in the vertical plane. Also, particles originating from the beam within the IMU steel have no additional shielding to prevent them from contaminating the plug and endwall calorimeters.

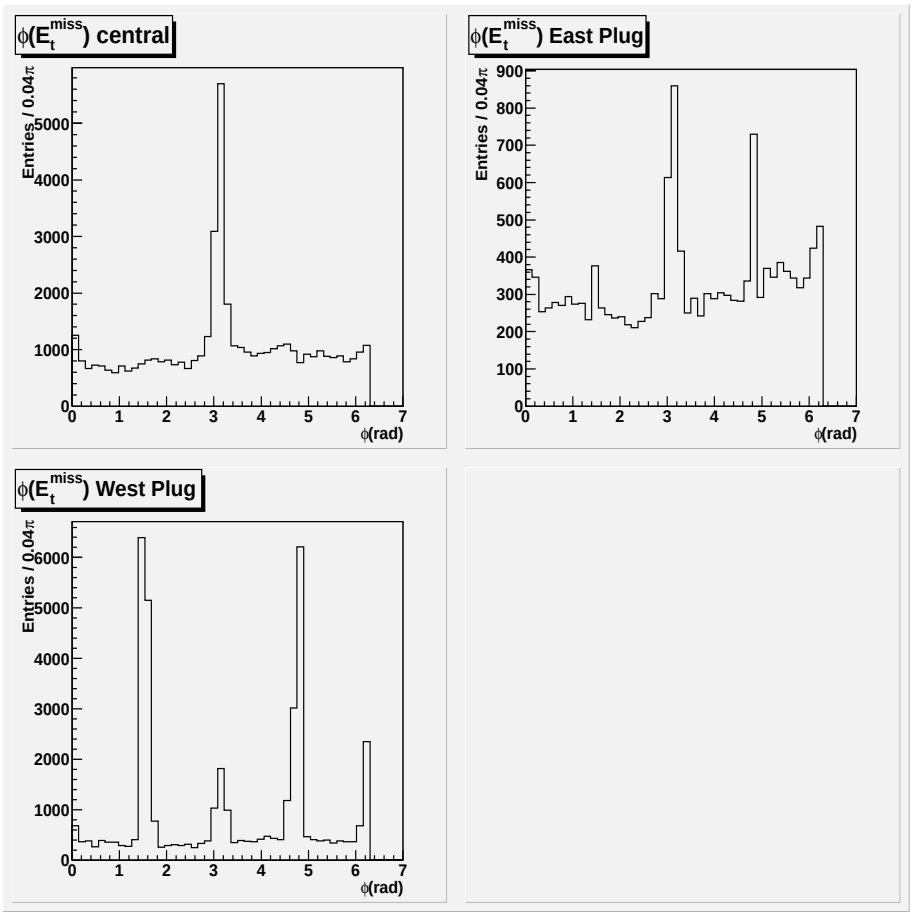

Figure 16: ϕ distribution for the missing E_T for the central and plug CDF calorimeters.

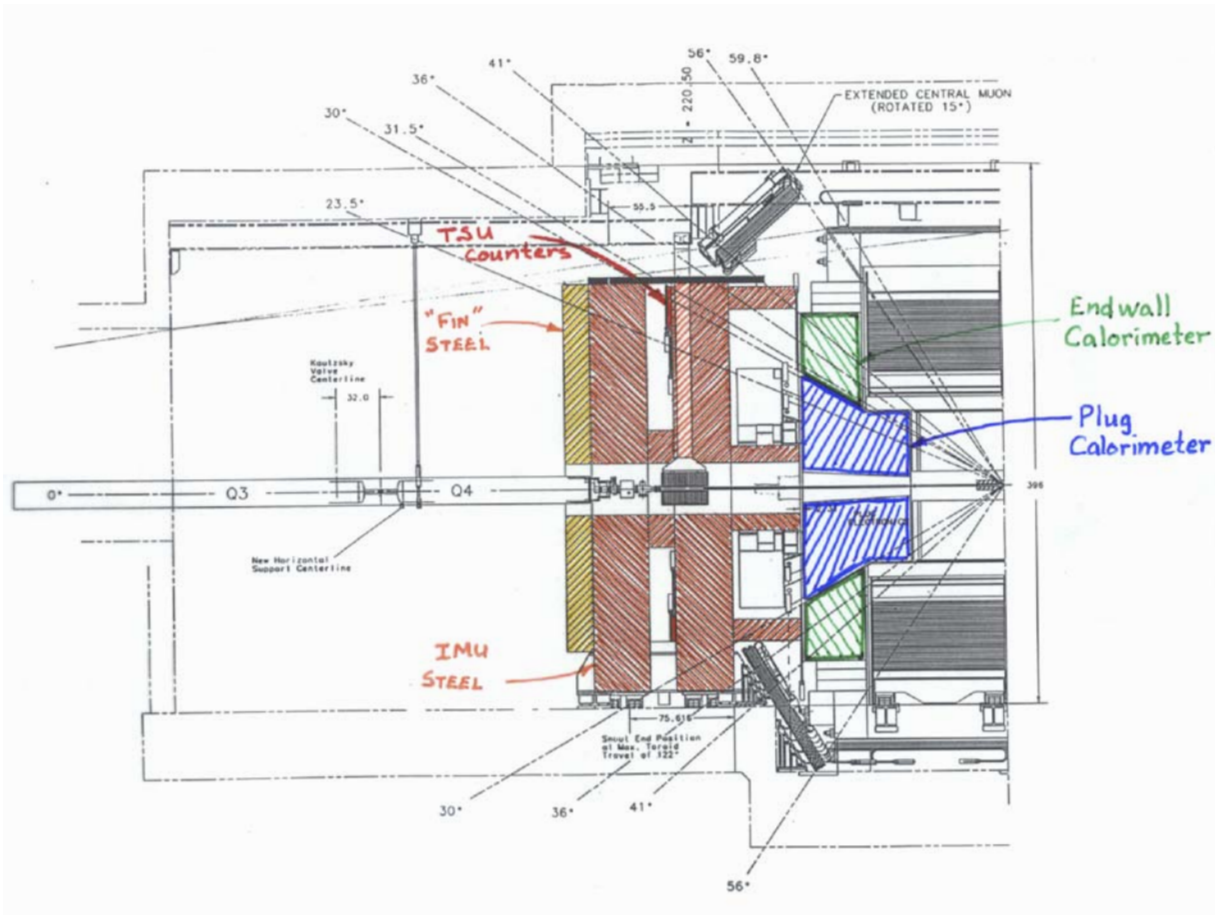

Figure 17: Vertical cross section of the CDF detector, collision hall and nearby beam line. Note the relative thickness of the shielding "Fin" compared with the other intermediate muon (IMU) shielding. Protons enter from the left.

3.2 Proton-only Stores

One can see from Figure 11 that besides the prominent peak at $\phi \approx 180°$ for the missing E_T, there are two small peaks at $\phi \approx 90°$ and $\phi \approx 270°$. We see prominent peaks as well at those locations in Figure 16. While investigating the beam halo as a function of the position of the roman pots, on March 26 we took a proton-only store (store 1130) with a single proton bunch in the machine. For run 141683 in this store we show the ϕ distribution of the missing E_T in Figure 18. We see a significant peak at $\phi \approx 90°$ and a less significant peak at $\phi \approx 270°$.

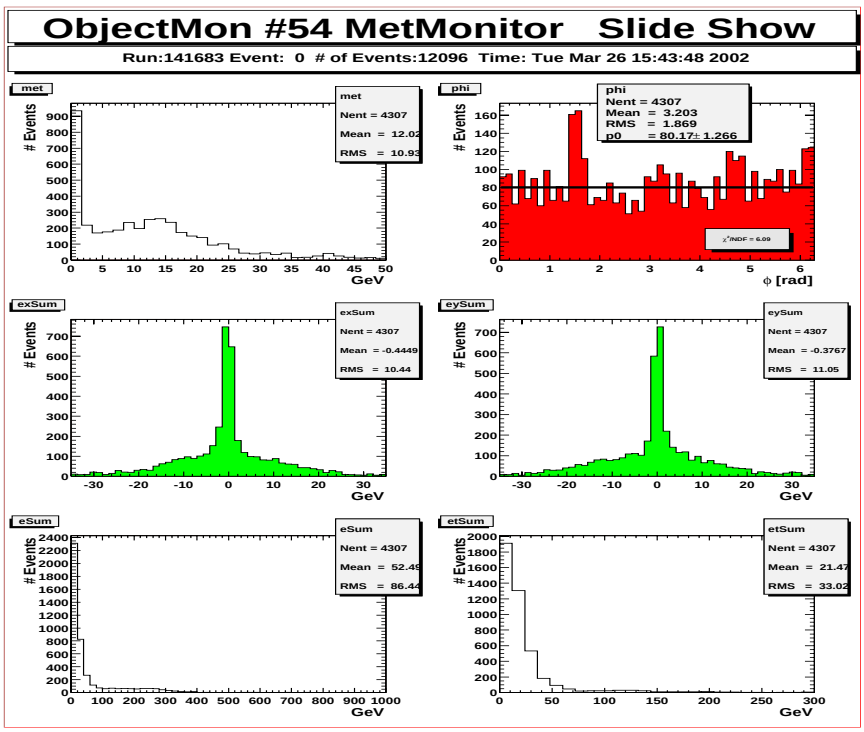

Figure 18: Various distributions for events satisfying the missing E_T trigger for a proton-only store, Run 141683. The roman pots are OUT.

On May 7 we took another proton only store (store 1295) and took data

with the default trigger table, where instead of triggering on the coincidence of West and East CLC we triggered on East CLC only ("East Diffractive"). In Figure 19 we show a few distributions at the trigger level for events satisfying the missing E_T trigger for the above store, run 144484. The ϕ distribution of the missing E_T exhibits again prominent peaks at $\phi \approx 90°$ and $\phi \approx 270°$. We also notice that the E_{tx}-E_{ty} distribution exhibits a characteristic "cross" shape.

In Figure 20 we show the E_{tx}-E_{ty} distribution from the same proton-only store reconstructed offline and for the highest η tower in the East plug calorimeter. We see a characteristic "cross" shape distribution with more activity in the vertical direction of the "cross". In Figure 21 we show the same distribution for the highest η tower of the West plug calorimeter. In Figure 22 we show a similar distribution for both the East and West plug calorimeters excluding the highest η towers.

In Figure 23 we show the plug energy distribution of events for which $|E_{ty}| < 5$ GeV or $|E_{tx}| < 5$ GeV, that is for the vertical and horizontal sections of the "cross". We see that these events are quite energetic.

In Figure 24 we show the t_0 distribution for events at the horizontal and vertical sections of the E_{tx} vs E_{ty} "cross" at the East and West plug calorimeters. The t_0 in the East has a mean of about 4 to 5 ns while the t_0 in the West has a mean of about -18 to -19 ns. The time difference between West and East is consistent with the distance between the West and East faces of the Plug/Endwall calorimeters. It is also clear that these events are coming from the West.

In Figure 25 we show the transverse energy in the West plug calorimeter for transverse energy in the East plug greater than 1 GeV (top) or less than 1 GeV (bottom). In Figure 26 we show the transverse energy in the East plug calorimeter for transverse energy in the West plug greater than 1 GeV (top) or less than 1 GeV (bottom). One can see that the West plug is actually hit more when there is not much energy in the East plug. One can also see that the East plug is hit more when there is not much energy in the West. So, from this it looks like that there is negative correlation between the East and the West.

These distributions might indicate that the particles producing the characteristic ϕ peaks in the missing E_T distribution in this proton-only stores "graze" the West plug calorimeter, go through the tracking volume of the CDF detector and land at the highest η towers of the East plug calorime-

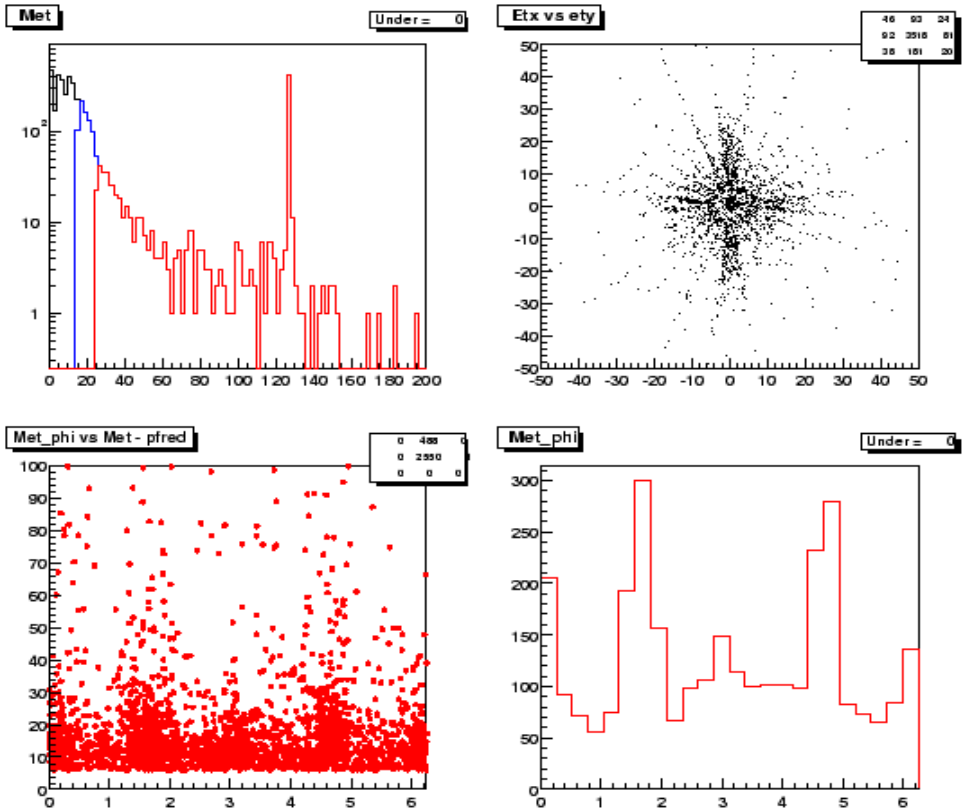

Figure 19: Various distributions at the trigger level for events satisfying the missing E_T trigger for a proton only store, run 144484. The top-left plot shows the missing E_T distribution in GeV. The spike around 120 GeV reflects saturation in the "cratesum" trigger quantity. The top-right plot shows the E_{tx}-E_{ty} distribution in GeV. The bottom-left plot shows the missing E_T in GeV vs ϕ in rads. The bottom-right plot shows the ϕ distribution of the missing E_T in rads.

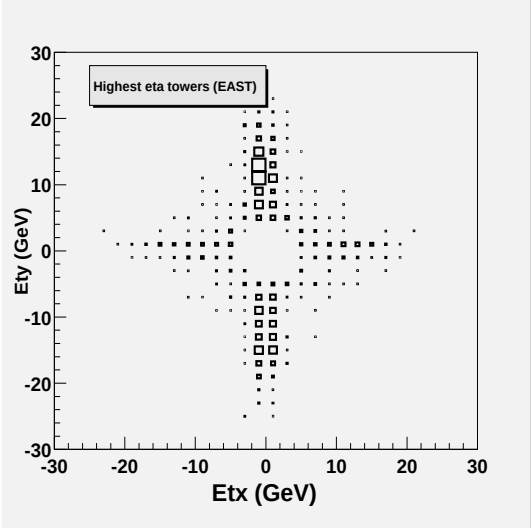

Figure 20: E_{tx} vs E_{ty} distribution for the highest η tower of the East Plug calorimeter.

ter. (Note that the highest η towers are the ones closest to the beam). It could also be likely that we have backgrounds from the beam hitting the East and West plugs independently. Another possible explanation for the disagreement we see between collision data and proton-only store data could be that the beam conditions are different for the proton beam between collision and proton-only stores. Based on the information we have so far[3], store 1130 was not close to HEP store conditions while store 1295 replicated HEP conditions very well (on helix, separators ON, etc.).

4 Conclusion

CDF is experiencing significant beam halo related background in the collision hall in Run II. Central calorimeter missing E_T spikes appear to be muons

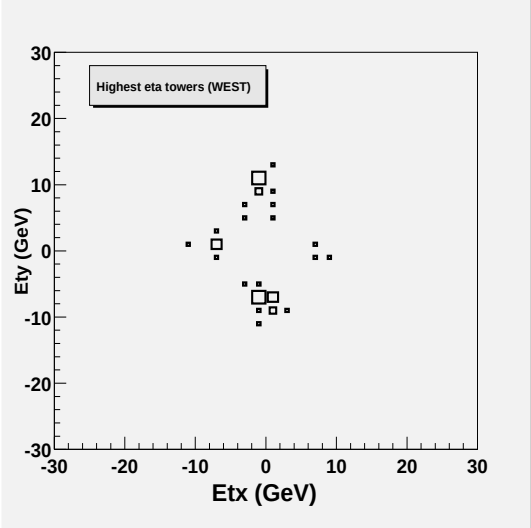

Figure 21: E_{tx} vs E_{ty} distribution for the highest η tower of the West Plug calorimeter.

originating from the region of the roman pots. We find a high degree of correlation in the missing E_T spike rate (but not the uniform in ϕ background) with pot position. This is likely due to the halo surrounding the proton beam hitting the detectors associated with the roman pots. The plug calorimeter missing E_T spikes during collision data appear to originate from beam losses. The plug calorimeter missing E_T spikes during proton-only store data are still under further investigation. We are working closely with the Beams Division in order to understand and minimize the background and we are in the process of evaluating several actions that can be taken.

5 Comments on Beam Halo - Plans

The large missing E_T trigger is clearly sensitive to interactions of proton beam halo in the beam pipe and in the roman pots, especially when the latter are fully inserted. These interactions may have other deleterious effects, such as causing high currents in the CMP and CMX chambers and noise hits in the

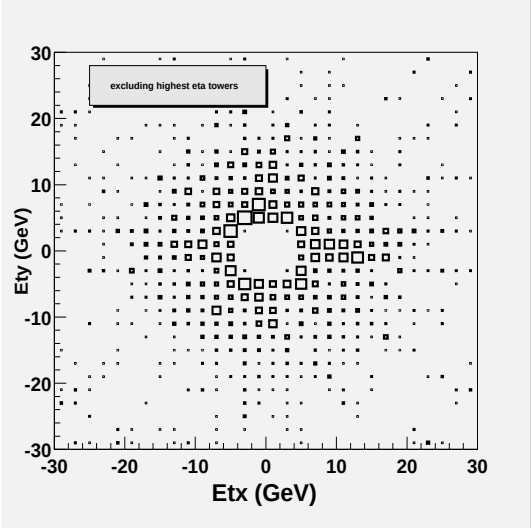

Figure 22: E_{tx} vs E_{ty} distribution excluding the highest η tower of the East and West Plug calorimeter.

COT. A study group of people from Beams Division, CDF and D0 meets regularly to address these issues [2] and one can find additional information on the issues discussed below at the WEB page of the study group referenced above.

The primary problem is halo generation by e.g. beam-gas interactions and intrabeam scattering. Beam gas interactions have already been reduced since the studies reported here, by improving the vacuum sector in F11 where there was a pressure bump. The proton beam halo was reduced by a factor of ∼6-8; this is still being studied and further reduction may be possible but some causes (e.g. intrabeam scattering) are irreducible.

The next problem is halo removal. This is done by systems of collimators. Experiments have been done varying their configuration but no significant (better than 10%) improvements were found. An interesting proposal is to use a bent silicon crystal instead of the 5 mm tungsten primary collimator. Calculations estimate that this could be more efficient at halo removal, and a proposal is being made to try this in the Fall of 2002.

The next issue is to minimize the effect of halo interaction products in

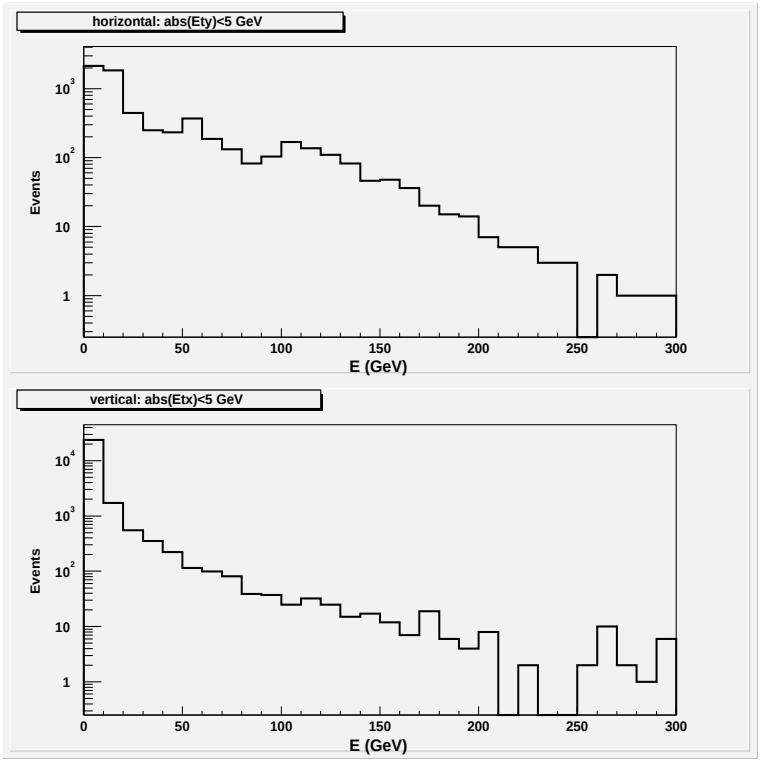

Figure 23: Energy distribution for events populating the horizontal (top) and vertical (bottom) sections of the E_{tx} vs E_{ty} "cross".

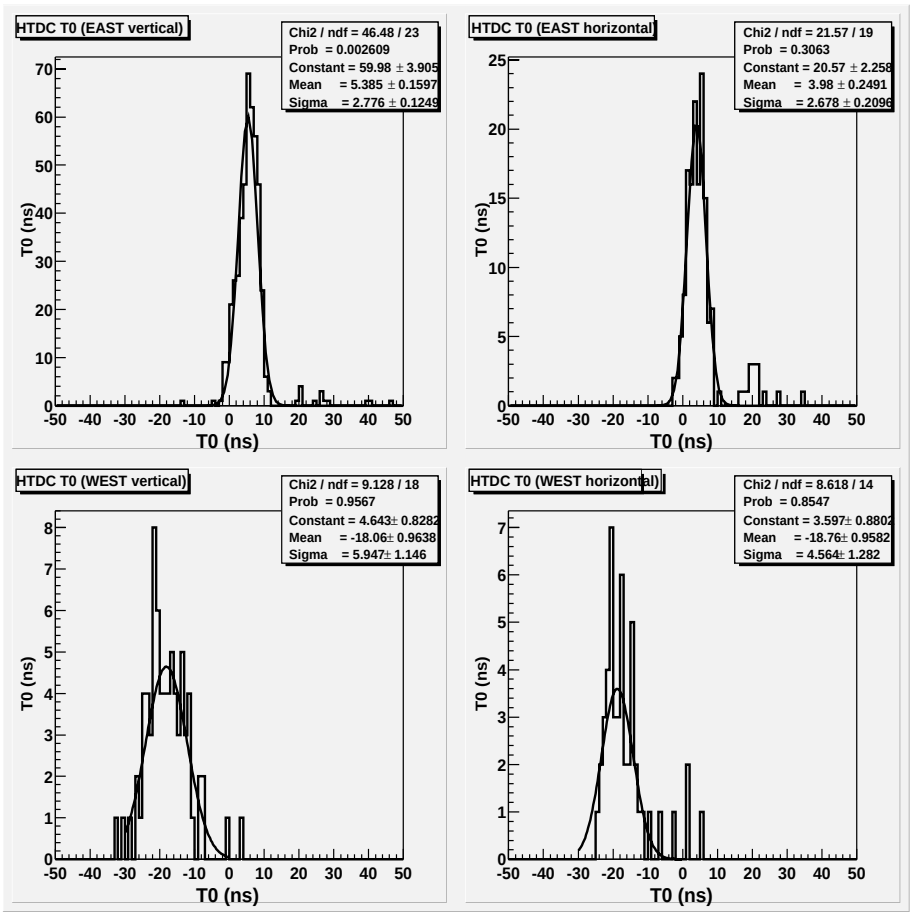

Figure 24: The t_0 distribution in ns measured from the TDCs of the hadronic calorimeters.

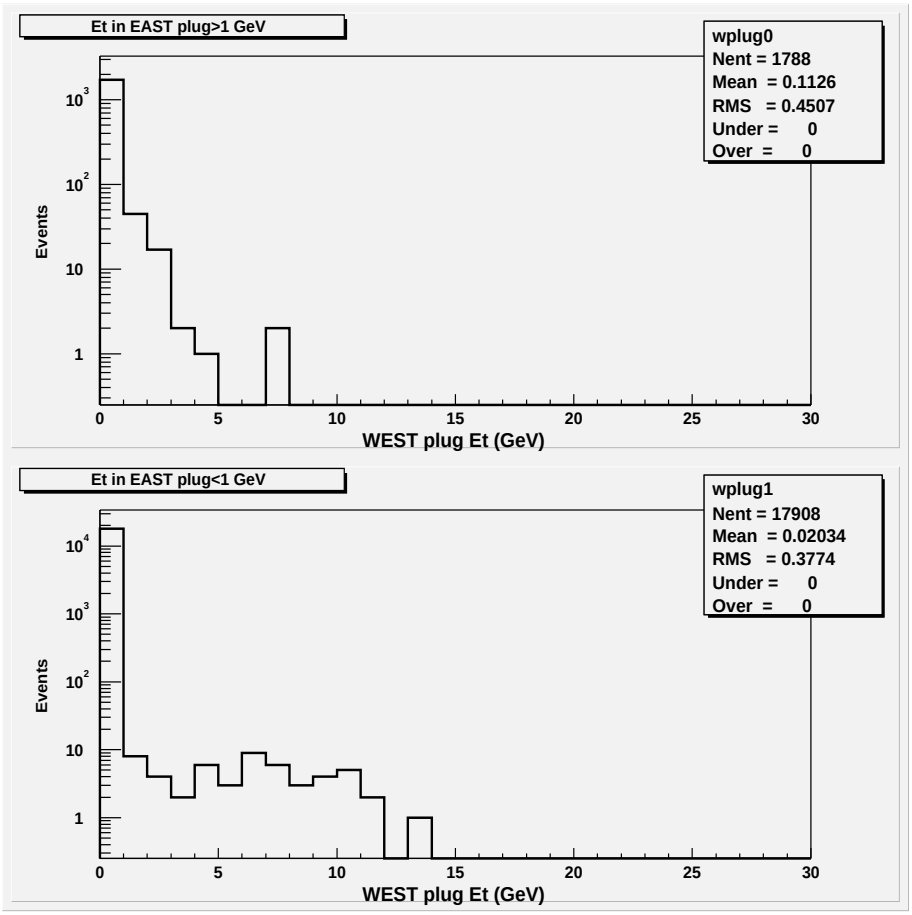

Figure 25: E_T in West plug calorimeter for E_T in the East plug greater than 1 GeV (top) or less than 1 GeV (bottom).

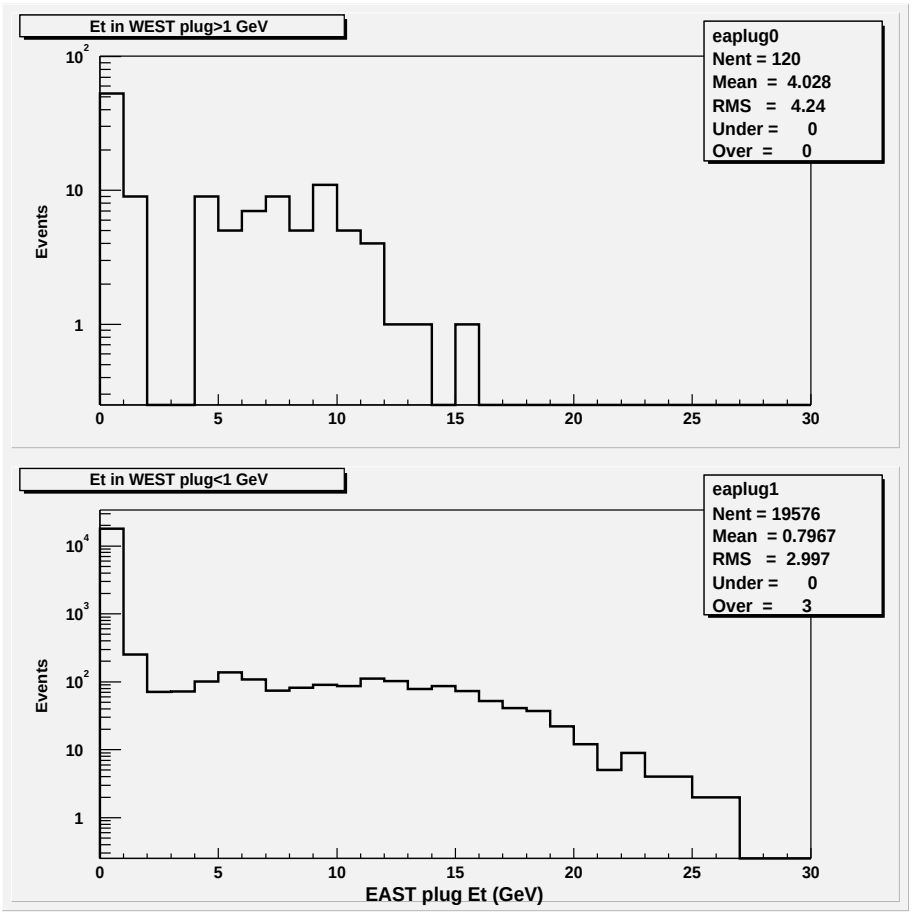

Figure 26: E_T in East plug calorimeter for E_T in the West plug of greater than 1 GeV (top) or less than 1 GeV (bottom).

CDF. The roman pots will not be fully inserted but run at ~ 0 mils where the halo is much reduced (see Figures 13, 15 and 27-29) until future improvements make this unnecessary. The shielding can and should be improved, especially in the vertical "crack" between the toroids and it would be useful to estimate the gain by comparing a simulation of beam-halo interactions with current data.

Finally the background affecting large missing E_T physics can be minimized by algorithms and cuts, as these energy deposits are very different from normal jets or photons. Some distinguishing features are the ratio of electromagnetic over hadronic energy, the $\eta - \phi$ shape of the showers (very elongated in η), the timing signals from the hadronic calorimeters and the absence of tracks pointing to the energy clusters. Note also that the probability of an energetic halo deposit superimposed on a genuine hard interaction is low ($\leq 10^{-6}$). (Rate $\sim$40 nb (Figure 15) $\times$ 5 E31 cm^{-2}s^{-1} = 2 s^{-1} with 2.5 10^6 crossings per second.) On the other hand a halo deposition superimposed on a minimum bias event could be mistaken for a photon+missing E_T event, if the above cuts cannot distinguish photons from halo.

6 Appendix: Roman Pot Scan of August 1st 2002

Another study of large missing E_T rates as a function of roman pot position was done on August 1st to compare with that done on April 1st (which was before the improvement in F11 vacuum). Figure 27 shows the MET45 rate as a function of the (approximate) positions of the 3 pots. The general level is reduced by about 30%, except for the position marked "fully in" where it has increased by 33%. Possible explanations are that while the halo has a lower tail it has a higher core, which seems unlikely, or that the proton beam and/or the pots are at a different x-position. It happens that while pots 1 and 3 had nearly the same position (LVDT) readings in the two runs, pot 2 was 1.09 mm closer to the beam (according to the LVDT) (see Figure 28). Given the steeply falling distribution, that is the likely explanation which can be checked in another short study. We also need to understand how possibly different luminosity conditions in the two stores might affect the trigger cross sections. Figure 29 shows the data divided into the $\phi \approx 180°$ peak and the flat (in ϕ) component. This can be compared with the same April 1st distribution, Figure 15. Both are seen to be independent of pot position until they are nearly fully IN ($\geq +100$ mils) when the $\phi \approx 180°$ peak increases dramatically. At the present default running position (~ 0 mils) very little effect is seen.

Another observation is that when the pots are moved in from their garage position in steps, the antiproton halo counters peak briefly and then decrease on a time scale of about 10 minutes. The counters are acting as collimators for the antiprotons. The effect on the proton halo is not clear, if any it is in the noise. We still have several questions and issues to investigate but we did not want to delay this note which hopefully will stimulate contributions. These questions include:

1) What was the missing E_T cross section and its ϕ distribution in Run 1, and was there a difference between Run 1B (before the pots were installed) and Run 1C (when they were in)?

2) What is the real expected cross section (and its missing E_T dependence) from full event and full detector simulation with all standard model pro-

cesses included? For example, what is the contribution from muons where they are not measured, e.g. in the forward region, and from "cracks" in the calorimeter?

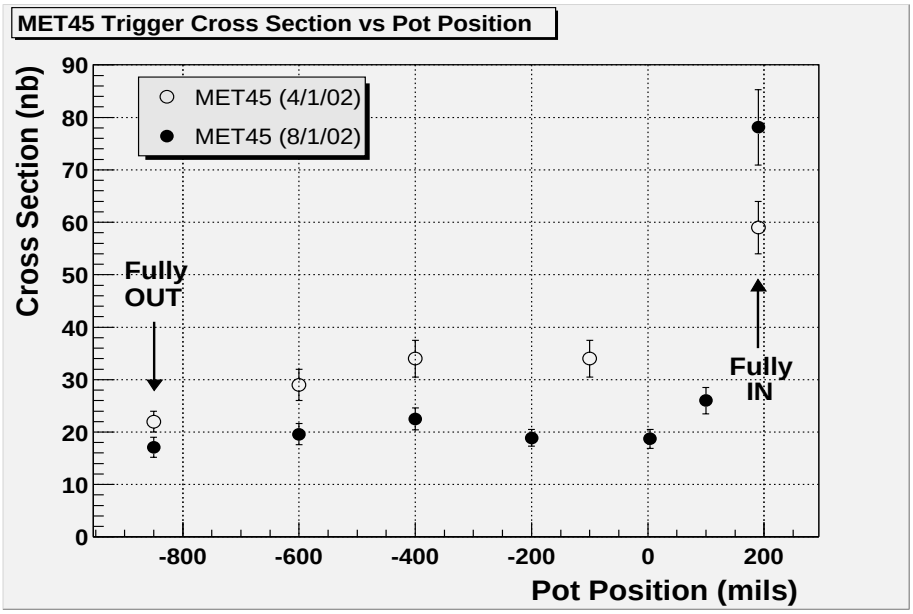

Figure 27: Cross section (integrated over ϕ) in nb for the $MET45$ trigger vs pot position for the April and August roman pot position scans.

August 1, 2002

MET Trigger Rate Scan with CDF Pots

Run#	Roman Pots (mils)			MET45 Trigger		B0 Lum	LOSTP	LOSTPB	#p	#pbar
	Pot-1	Pot-2	Pot-3	σ (nb)	Rate (Hz)	(E30)	(kHz)	(kHz)	(E12)	(E11)
4/1/2002 (store# 1152)										
142202	-864	-853	-854	22.0	0.12	3.4	18.8	1.5	6.7	1.4
142206	-600	-600	-600	29.2	0.09	3.1	17.5	1.5	6.7	1.3
142205	-397	-399	-398	33.7	0.11	3.2	17.8	1.5	6.7	1.4
142204	-100	-100	-100	33.6	0.11	3.2	18.0	1.5	6.7	1.4
142203	+176	+192	+215	58.6	0.20	3.3	17.5	1.5	6.7	1.4
8/1/2002 (store# 1613)										
149269	-872	-898	-857	17.1	0.10	5.8	7.2	1.0	4.7	2.4
149279	-605	-605	-605	19.6	0.11	5.7	7.0	0.90	4.7	2.4
149280	-400	-401	-399	22.5	0.12	5.7	7.0	0.93	4.7	2.4
149282	-197	-198	-197	18.9	0.10	5.5	6.8	0.90	4.7	2.4
149283	+5.0	+2.5	+4.2	18.7	0.10	5.4	6.4	0.87	4.7	2.4
149287	+99	+100	+98	26.0	0.13	5.1	6.2	0.85	4.7	2.4
149284	+177	+235	+206	78.1	0.49	5.3	6.8	0.85	4.7	2.4

Figure 28: Pot positions and trigger cross sections for the April and August roman pot position scan.

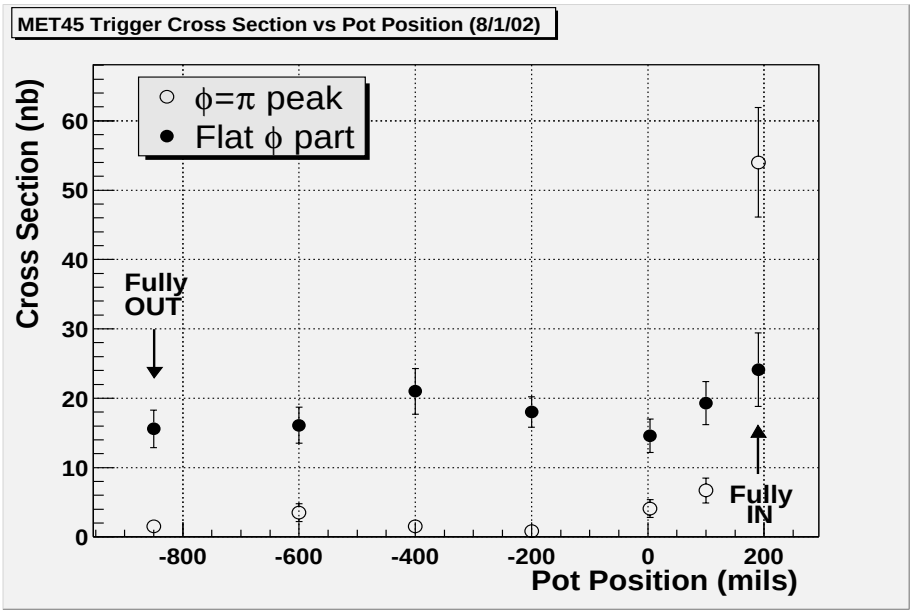

Figure 29: Cross section in nb for the $MET45$ trigger vs pot position for the August roman pot position scan. The white circles correspond to the $\phi \approx 180°$ peak. The black circles correspond to all other angles.

References

[1] D. Glenziski et al., "Determination of the COT tracking efficiency using the W-No-Track sample", CDF/PHYS/ELECTROWEAK/CDFR/5973

[2] http://home.fnal.gov/ maeshima/halo/halo.html

[3] Ron Moore, private communication.